Journal of Nuclear Materials 618 (2026) 156233

Contents lists available at ScienceDirect

Journal of Nuclear Materials

journal homepage: www.elsevier.com/locate/jnucmat

High heat flux testing of plasma-facing component mock-ups with tailored tungsten-copper composite heat sinks

R. Lürbke [a,b,*], A. von Müller [b], B. Böswirth [b], B. Curzadd [b], H. Greuner [b], J. Riesch [b], G. Schlick [c], R. Neu [a,b]

[a] Technical University of Munich, Garching, 85748, Germany
[b] Max Planck Institute for Plasma Physics, Garching, 85748, Germany
[c] Fraunhofer Institute for Casting, Composite and Processing Technology IGCV, Augsburg, 86159, Germany

ARTICLE INFO

Keywords:
Tungsten
Copper
Additive manufacturing
High heat flux
Plasma-facing component
Metal-matrix composite

ABSTRACT

Plasma-facing components (PFCs) in future magnetic confinement fusion reactors must sustain high heat fluxes and intense neutron irradiation. These extreme conditions demand specially engineered material solutions. State-of-the-art designs for highly loaded PFCs are based on bulk tungsten (W) armor combined with a copper (Cu) alloy heat sink. Whereas the monoblock design cannot be readily extrapolated to large dimensions due to the large number of armor blocks, the broader use of the flat-tile design is limited due to concerns about the integrity of the joint of the armor to the heat sink, i.e. the delamination of armor tiles. Therefore, a material design is being explored in which tailored tungsten-copper (W-Cu) composite structures are utilized to minimize thermally induced stresses and to strengthen the bond between a W armor and a Cu based heat sink. These composites are based on W lattice-like preforms, which are additively manufactured utilizing laser-based powder bed fusion (PBF-LB) on monolithic W armor tiles. The composite is created in a vacuum-assisted Cu melt infiltration process. The present work summarizes investigations on two composite specimens with different honeycomb-type W lattice preforms. High heat flux tests were performed in the GLADIS facility to assess the behavior and the thermomechanical response under cyclic heat loading procedures up to 500 pulses at $20\,\mathrm{MW\,m^{-2}}$ surface heat load. No deterioration in the heat removal capability of the composite heat sinks was found throughout the cyclic tests. Although further optimization of the composite fabrication process is still necessary, the results can be considered a strong hint for the superior performance of the presented PFC concept.

1. Introduction

One of the major challenges for the realization of future magnetic confinement fusion power plants is the development and qualification of suitable materials and designs for highly loaded in-vessel plasma-facing components (PFCs) [1]. The maximum heat fluxes such wall components can withstand limit the overall performance of fusion devices and the reachable plasma scenario [2]. Tungsten (W) is considered the preferred plasma-facing material (PFM) for PFCs due to its high threshold energy for hydrogen isotope sputtering, low hydrogen isotope retention, and high melting point [3,4]. Copper (Cu) and Cu alloys, in particular the precipitation hardenable Cu alloy CuCr1Zr, are considered the preferred heat sink materials for highly loaded PFCs since they exhibit a very high thermal conductivity [4,5].

Traditionally, two main PFC designs for the highly heat-loaded divertor region in magnetic confinement fusion devices have been researched. Both designs are schematically shown in Fig. 1. On the one hand, the so-called monoblock design comprises monolithic W blocks bonded to a circular CuCr1Zr cooling pipe [6–9]. The monoblock design exhibits good damage resilience, but defects have for example been observed along the W-Cu interface after several hundred pulses at $20\,\mathrm{MW\,m^{-2}}$ surface heat load due to fatigue induced by the thermal expansion mismatch between the W blocks and the CuCr1Zr tube [10]. Also, during extensive high heat flux testing at $20\,\mathrm{MW\,m^{-2}}$ for the ITER divertor program, the monoblock design showed tendencies for deep cracking [11,12]. It is to be noted that all tests mentioned above were performed without taking into account effects of neutron irradiation on the tested PFC mock-ups.

* Corresponding author at: Max Planck Institute for Plasma Physics, Garching, 85748, Germany.
E-mail address: robert.luerbke@ipp.mpg.de (R. Lürbke).

https://doi.org/10.1016/j.jnucmat.2025.156233
Received 31 January 2025; Received in revised form 10 July 2025; Accepted 16 October 2025

Available online 17 October 2025

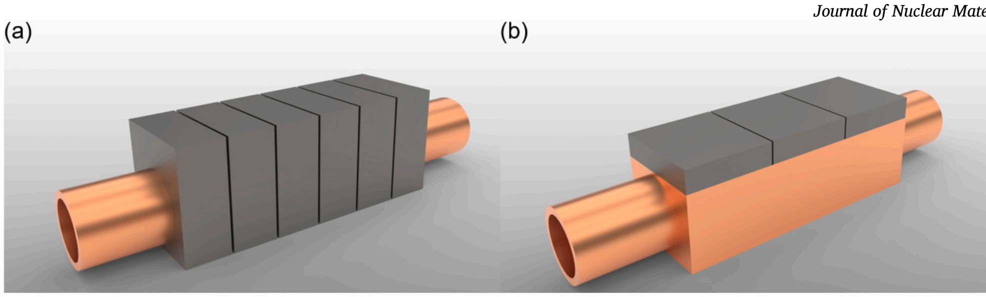

Fig. 1. Traditionally researched PFC designs. (a) Monoblock design with W blocks bonded to a Cu alloy heat sink pipe. (b) Flat-tile design with a Cu alloy heat sink block and W armor tiles bonded to it.

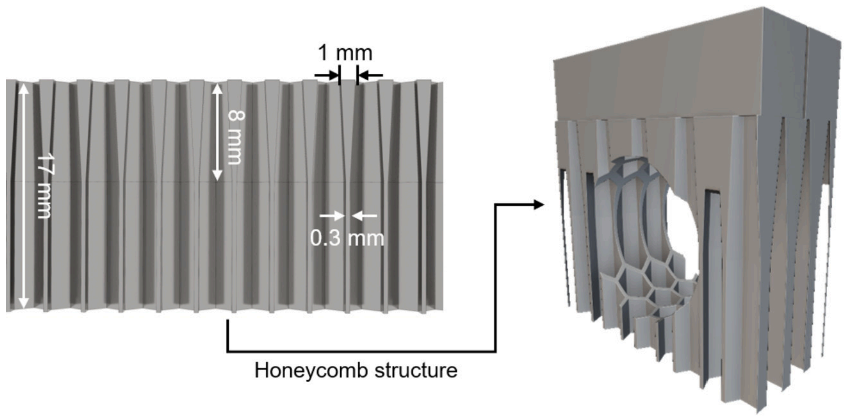

Fig. 2. 3D CAD model of the heuristic design. The gradient in W volume fraction is realized by a 8 mm long section with a linear gradient, which then continues in a non-graded extrusion.

On the other hand, the so-called flat-tile design is an actively cooled Cu heat sink block with castellated W armor tiles bonded to its plasma-facing side [6]. However, singular stress concentrations occur in such a design during thermomechanical loading at the free surface edges of the material joints. These stress concentrations lead to issues regarding the integrity of the W-Cu joint and may lead to a complete failure of the component, for example, due to delamination of entire armor tiles [13–16].

The present paper summarizes investigations regarding the manufacturing and testing of a novel material concept that tries to mitigate the PFC design issues mentioned above. This is achieved by improving the bonding between the armor tiles and the heat sink as well as optimizing W and Cu material distributions in the heat sink part of the PFC. The goal of this optimization is to minimize the thermally induced stresses under high heat flux loading. Additive manufacturing (AM) is exploited due to its design freedom to realize such tailored material distributions in the composite. The two materials are combined in a metal-matrix composite (MMC) based on additively manufactured W preforms, which are infiltrated with Cu during a melt infiltration process.

2. Tailored material distribution in plasma-facing components

The work presented in this paper assesses two specimens based on W honeycomb lattice preforms. The first type of preform is created based on a heuristic approach. This design comprises two sections, one with a graded wall thickness and a second with a constant wall thickness. The linear graded section is 8 mm high and varies from 1 mm to 0.3 mm in wall thickness. The graded section is continued in a section with a 9 mm long wall with a constant thickness of 0.3 mm. The unit cell size of the lattice is 2.5 mm. A 3D computer-aided design (CAD) model of the part is shown in Fig. 2.

The second type of preform is a computationally optimized honeycomb-type lattice. The optimization is based on the *MSPFC* (Minimum Stress in Plasma-Facing Components) code developed by Curzadd et al. [17]. This code utilizes a finite element (FE) method to describe the thermo-mechanical behavior of a two-phase composite material. The material models for the code are based on a numerical homogenization approach, meaning that the macroscopic properties of a composite are determined by spatially averaging unit cells of a lattice structure. This structural optimization technique uses temperature-dependent material models to minimize the peak von Mises stresses in the component for a given surface heat flux and stress-free temperature. Predictions of a 2D case indicate a possible stress reduction of up to 85% compared to a plain bulk W block [17].

In the layerwise optimization performed for the present work, the *MSPFC* code is applied to a 1D problem. This is achieved by keeping material volume fractions constant in layers with a fixed height of 1 mm. As boundary conditions, the top 5 mm of the component is set to a W volume fraction of 100% to represent the armor. The incident heat flux is chosen to be $20\,\mathrm{MW\,m^{-2}}$ and the stress-free temperature is set to 1050 °C, which corresponds approximately to the solidification temperature of Cu. After optimization, the design space shows a gradient in W content. Fig. 3 shows the iterative optimization's first and last steps, comparing the initial W volume fraction and von Mises stress to the optimized state. Due to the optimization, the peak von Mises stress in the part is reduced.

In Fig. 4, the result of the optimization is displayed next to the corresponding 3D model created in a CAD software. The unit cell size of the lattice is 2.5 mm. The lines from the discretization of the layered optimization result are visible in the model.

3. Additive manufacturing of optimized PFC W preforms

The W preforms are manufactured by an AM process called laser beam-based powder bed fusion (PBF-LB) [18]. The W powder raw material used in this work is *TEKMAT W-25* supplied by *Tekna Advanced Materials Inc.* (Québec, Canada). This powder grade was found to yield good build results in PBF-LB due to its high spheroidicity and low oxy-

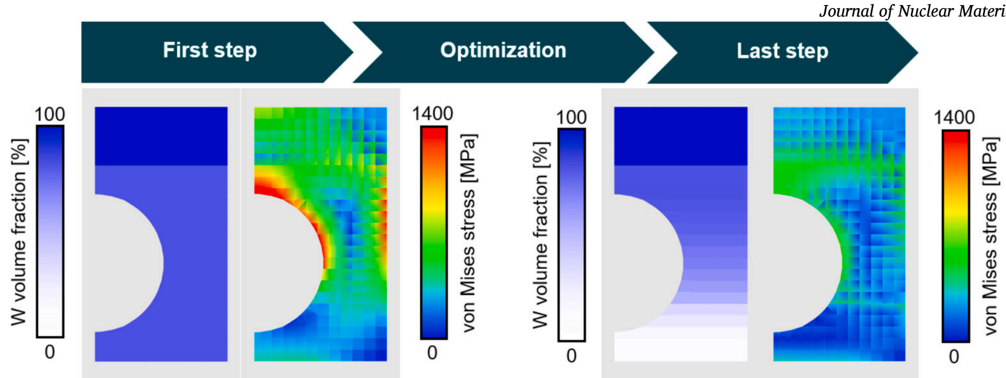

Fig. 3. First and last step of a layer-by-layer optimization with the MSPFC code developed by Curzadd et al. [17]. The first step is the starting condition, where a W volume fraction of 100% is set for the armor and a constant W volume fraction of 70% is set for the heat sink. After optimization, the structure shows a gradient with 0% of W at the part's lower section.

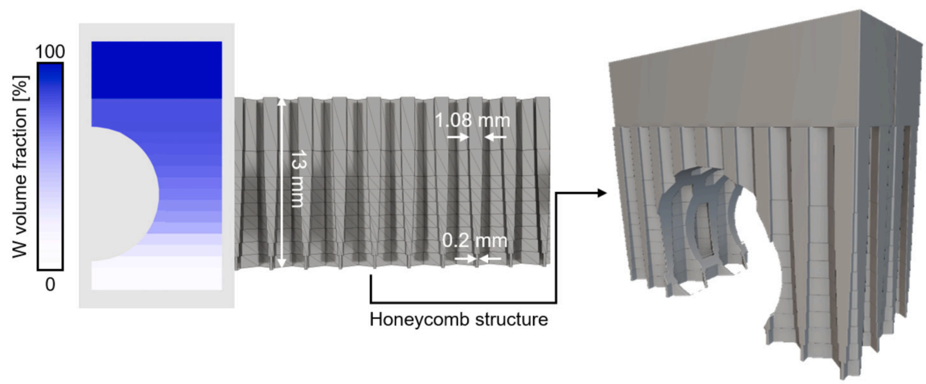

Fig. 4. Result of the optimization and the corresponding design of the honeycomb lattice. The discrete steps in the layer-by-layer optimization can be seen in the 3D CAD model.

gen content [19]. The specified particle size distribution of *TEKMAT W-25* has a D10 of 5 µm and a D90 of 25 µm. [20]

An *AconityONE* PBF-LB machine made by *Aconity3D GmbH* (Aachen, Germany) is used at the *Fraunhofer Institute for Casting, Composite and Processing Technology IGCV* (Augsburg, Germany) to manufacture the preforms investigated in the present work. For the preform fabrication, the laser power is set to 400 W, the hatch distance is set to 80 µm, and the layer height is set to 40 µm. A laser scanning speed of 570 mm s^{-1} is used for the consolidation of the optimized preform, while the heuristic preform is built with a laser scanning speed of 510 mm s^{-1}. Furthermore, the pre-processing of the CAD file for the heuristic preform was performed manually. This might also explain differences in the material quality between the heuristic and optimized preforms. The W build plate temperature is 600 °C. Wire-cut electrical discharge machining (EDM) is used to remove the samples from the build plate.

Fig. 5 shows scanning electron microscopy (SEM) images of micrographs of the two investigated preforms.[1] The white boxes in the overview images indicate the locations where the SEM images were taken. The optimized design preform (Fig. 5b) shows little porosity and some cracking along the columnar grain boundaries. The heuristic design preform (Fig. 5a) shows significantly bigger grains, as well as more pronounced porosity and significant intergranular cracks.

The anisotropic mechanical and fracture properties of rolled W plates used to fabricate PFC armor tiles are a decisive feature. Due to this anisotropy, their rolling direction must be aligned with the later heat flux direction [21]. Usually, the rolling direction of W plates used as a substrate in PBF-LB machines is oriented in-plane. To achieve the desired grain orientation in later PFC mock-ups, the W substrate is modified with recesses and set in W armor tiles cut from a grade 3N plate manufactured by *A.L.M.T. Corp.* (Tokyo, Japan). With this modification, W lattices can be directly built on W armor tiles. Fig. 6 shows the modified substrate and heuristic and optimized honeycomb lattices as-built. It is important to note that the heuristic mock-up tested in this work is built on an as-received W substrate, so the rolling direction of the armor tiles is not aligned with the heat flux direction. The optimized mock-up is built on a modified substrate, so the rolling direction of its armor tiles is aligned with the heat flux direction.

4. Vacuum assisted melt infiltration

The PFC mock-ups investigated in this work are produced using a vacuum-assisted melt infiltration process, where the AM preforms are filled with Cu to create a MMC. In this process, the W preforms produced by PBF-LB are placed in crucibles made from hexagonal boron nitride (α-BN) (*HeBoSint CL-Z 200* manufactured by *Henze BNP AG*, Lauben, Germany). α-BN is used because there are no undesired reactions at the process temperatures. The raw Cu material (grade CW009A) is procured as bars and machined to fit the crucibles. Before the materials are placed in the crucibles, the Cu bars are cleaned with 5% citric acid in water for half an hour in an ultrasonic bath. The W preforms are cleaned using the same process in a solution of 1.5% NaOH in water. Finally, the crucibles are thoroughly cleaned with isopropyl alcohol. Fig. 7 **(a)** shows an infiltration setup after cleaning and assembly.

The assembled infiltration setup is then placed in a *TZF 15/610* ceramic tube furnace manufactured by *Carbolite Gero GmbH & Co. KG* (Neuhausen, Germany). A stable infiltration procedure, which laid the foundation for the process used in our work, was developed in [22]. A maximum process temperature of 1150 °C is used to prevent extensive grain growth in the W armor tiles, and a holding time of 3 h is used to

[1] The samples were etched with Murakamiś reagent.

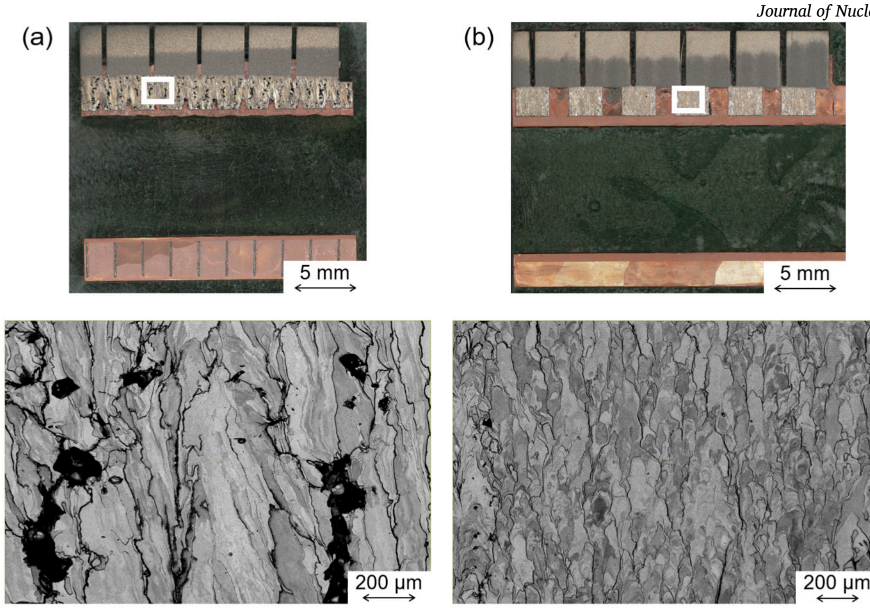

Fig. 5. SEM images of the AM W preforms, taken post-exposure. The white boxes in the overview images indicate the locations from which the SEM images were taken. **(a)** Heuristic design preform: The AM W shows pronounced porosity and cracks. **(b)** Optimized design preform: Some intergranular cracks are visible, while porosity and cracking are less pronounced than in the heuristic design preform.

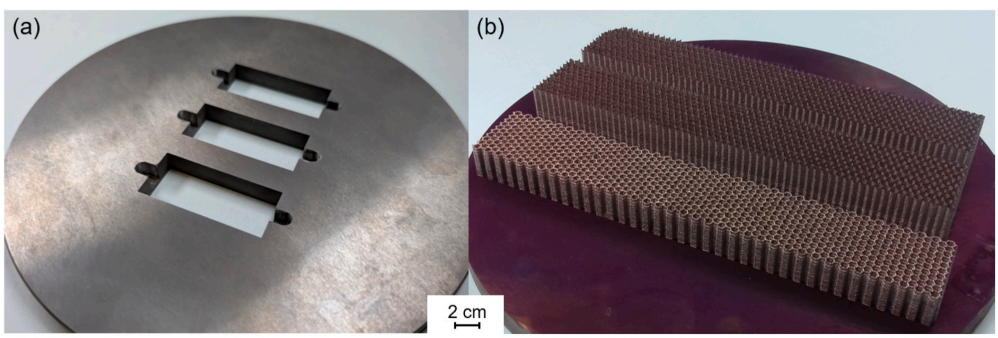

Fig. 6. (a) W substrate used in the *AconityONE* PBF-LB machine with machined recesses for W armor tiles. **(b)** Honeycomb lattice preforms produced by means of PBF-LB at *Fraunhofer Institute for Casting, Composite and Processing Technology IGCV* (Augsburg, Germany).

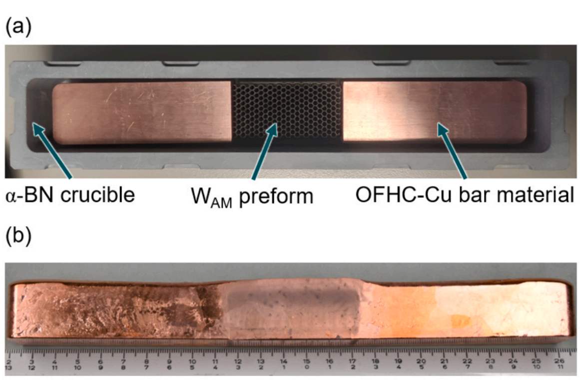

Fig. 7. (a) Top view of an AM W preform set into a α-BN crucible for infiltration. The Cu (CW009A) matrix material is placed in as solid bar material. **(b)** Side view of an ingot resulting from the melt infiltration process. The ingot is slightly bent due to the asymmetric material distribution.

allow for thorough penetration through the W preform. Furthermore, heating and cooling rates of 5 K min^{-1} are used. Before the cooling and solidification phase, the system is pressurized to atmospheric pressure with Ar gas to support the infiltration of the preform and thus reduce porosity in the Cu matrix according to [22]. The programmed temperature and pressure evolution during the process can be seen in Fig. 8.

Due to the slow cooling rate (set point 5 K min^{-1}) indicated in Fig. 8, the grains of the vacuum melt infiltrated Cu matrix typically grow to comparably large sizes. Fig. 9 shows an SEM image of the infiltrated Cu matrix taken from the region indicated with the white box in the overview image. The image shows the optimized mock-up after the high heat flux tests. The SEM image is taken from the non-loaded side of the specimen. As the infiltration process has been optimized for minimal porosity in [22], only small pores are visible.

As shown in Fig. 7 (b), the asymmetric material distribution in the composite billet causes it to bend slightly during the cooldown phase, so it has to be mechanically straightened to keep within the tolerances of the later processing steps. The small-scale mock-ups are then machined according to the dimensions illustrated in Fig. 10. To ensure leak tightness, the cooling channel outlets are precision turned and fitted with Swagelok tapered vacuum fittings. After manufacturing, the mock-ups are vacuum leak tested with helium gas. The test procedure starts with testing at room temperature and 4 MPa of pressure, followed by testing at 160 °C and 3 MPa, and concluded with a third test at 4 MPa after the samples have cooled down below 60 °C. The test is passed if the samples show a leak rate below 5×10^{-9} mbar l s^{-1} in all three steps. Initially, neither mock-up passed the vacuum leak test, so the inner side of the cooling channel was sealed using galvanic deposition of Cu at *Galvano-T electroforming-plating-GmbH* (Windeck, Germany). This electrochemically deposited Cu layer is also visible in the micrographs in

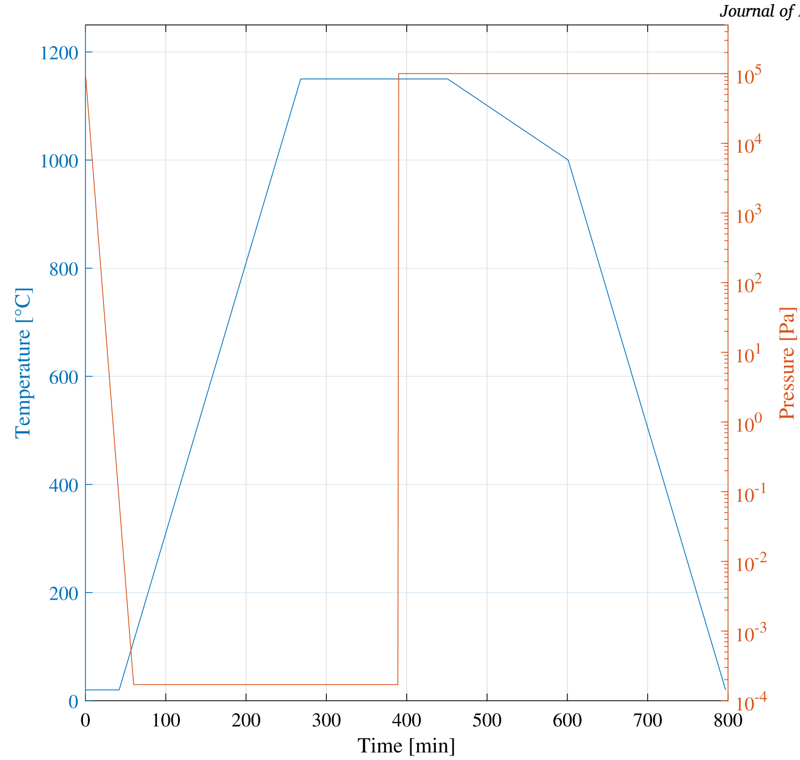

Fig. 8. Programmed temperature and pressure evolution during the vacuum-assisted melt infiltration. The molten Cu is re-pressurized with Ar gas to support the infiltration of the preform with Cu.

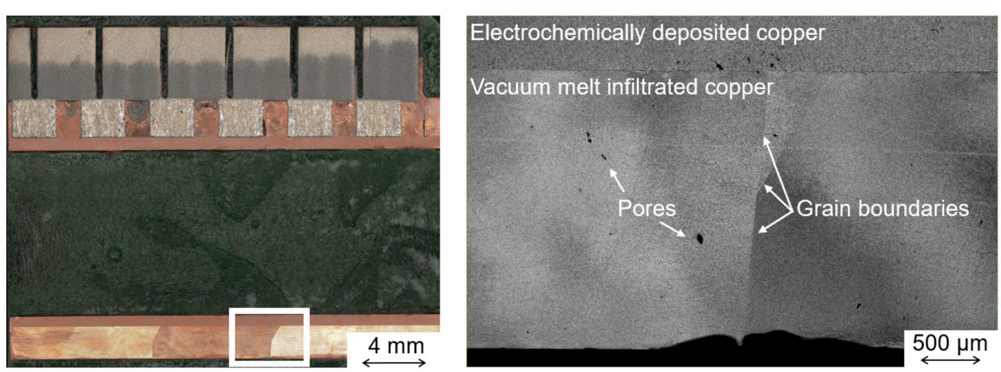

Fig. 9. SEM image of the Cu matrix material, taken from the area indicated by the white box in the overview image. The top of the SEM image shows electrochemically deposited Cu, which was added in the repair process. It is also visible in the overview image. The rest of the SEM image shows the vacuum melt infiltrated Cu. The slow cooling rate of 5 K min^{-1} causes the formation of large grains. Grain boundaries and pores in this image are indicated by the white arrows.

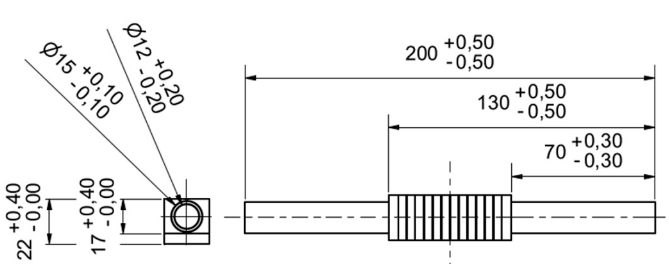

Fig. 10. Dimensions of the small-scale mock-ups, given in mm.

Fig. 9. The actual inner diameter of the mock-ups after the repair is 11 mm. The mock-ups passed the second vacuum leak test after the galvanic repair.

5. High heat flux testing

The high heat flux tests are performed with GLADIS (Garching large divertor sample test facility) at the Max Planck Institute for Plasma Physics [23,24]. Surface heat fluxes up to 25 MW m^{-2} are used, created by a 1 MW neutral beam source. A 1-color and a 2-color pyrometer are available for surface temperature measurements. The emissivity is set to $\epsilon = 0.3$ for the measurements of W surfaces with the 1-color pyrometer *Serie 740* from *Kleiber Infrared GmbH* (Unterwellenborn, Germany). The 2-color pyrometer *QKTRD 1075-1* from *Dr. Georg Maurer GmbH Optoelektronik* (Kohlberg, Germany) possesses a measuring range from 500 °C to 1700 °C. Since the results of the 2-color pyrometer are independent of the emissivity of the measured material, its measurements are preferred in the evaluation. Outside of this range, the values from the 1-color pyrometer will be given. The error on the surface temperature measurements is estimated with ± 5%. The high heat flux testing is divided into

Table 1
Overview of the high heat flux test procedures the small-scale mock-ups underwent. The pulse duration for all procedures is 10 s.

Procedure	Heat fluxes [$MW\,m^{-2}$]	Water inlet temperature [°C]	Pulse count
Screening	6, 8, 10, 15, 20, 25	20	3*
Cycling	10	20	100
Screening	6, 8, 10, 15, 20	130	3*
Cycling	20	130	500

* The 3 pulses were performed at each heat flux level.

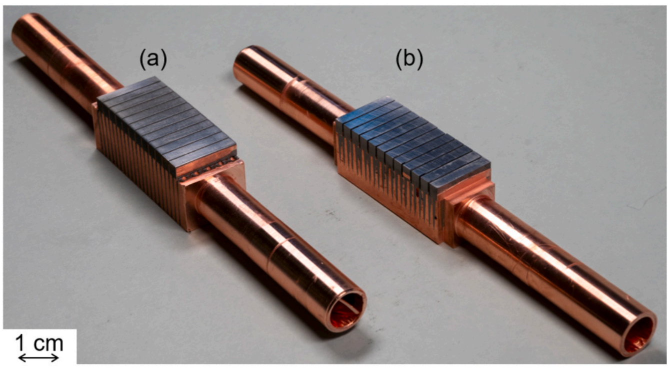

Fig. 11. Both small-scale mock-ups before high heat flux testing. (a) Mock-up with heuristic W preform. (b) Mock-up with optimized W preform.

two procedures. An overview of the procedures and the applied parameters can be found in Table 1. During screening, the thermal performance of the small-scale mock-ups at increasing heat fluxes is investigated. During the cycling tests, the fatigue behavior of the components under repeated high heat loads is assessed. The cooling water parameters in these procedures are 20 °C at 10 bar and 12 $m\,s^{-1}$ as well as 130 °C at 40 bar and 16 $m\,s^{-1}$. The cycling procedure at 20 $MW\,m^{-2}$, 130 °C water temperature and 500 pulses is a specified design criterion for the European DEMO [25,26]. Both specimens are equipped with 1 mm stainless steel swirl tapes [27] with a twist ratio of 2.8. Fig. 11 shows both mock-ups before the testing in GLADIS. The surface of the W armor tiles is honed with P600 honing paper before high heat flux testing.

Before the high heat flux tests were conducted, a non-linear static thermal finite element (FE) calculation is performed to assess the expected surface temperature values during cold-water screening at 20 $MW\,m^{-2}$. The set-up of the simulation in the computational design software nTop version 5.12.2 [28] can be seen in Fig. 12. At a cooling water temperature of 20 °C, the convection coefficient for the convection boundary condition is set to $1 \times 10^5\ W\,m^{-2}\,K^{-1}$. The W and Cu regions are separately meshed with an edge length of 0.3 mm and a growth factor of 2. The temperature-dependent material property data for both materials is taken from [29]. Since the MMC is created in a melt process, no gap can exist between the two materials, so the thermal resistance is set to near zero ($1 \times 10^{-13}\ m^2\,K\,W^{-1}$) and a ll radiative losses are neglected.

The results of the simulations for thermal equilibrium can be found in Fig. 13. The heuristic mock-ups design shows a calculated maximum surface temperature of 1515 °C, while the optimized mock-up shows a maximum temperature of 1595 °C. This difference in temperature is possibly caused by the difference in W volume fraction at the material joint between the heat sink and the armor tiles.

During screening with 20 °C cooling water, both mock-ups show a linear increase of surface temperature with incident heat flux as seen in Fig. 14. The surface temperature of the optimized mock-up is around 100 °C higher than that of the heuristic mock-up. The temperature differences in hot- and cold-water screening are consistent with the aforementioned FE calculations. No hot spots developed during screening up to 25 $MW\,m^{-2}$ on both samples. During cold water cycling at 10 $MW\,m^{-2}$, the heuristic mock-up shows surface temperatures of 820 ± 40 °C. The optimized mock-up shows temperatures of 915 ± 45 °C.

The screening with 130 °C cooling water yields analogous results to the cold water screening. The heuristic mock-up shows surface temperatures of 1610 ± 80 °C, while the optimized mock-up shows surface temperatures of 1660 ± 85 °C at 20 $MW\,m^{-2}$. During cycling at elevated cooling water temperatures, the heuristic mock-up shows increasing surface temperatures with increasing pulse number. This behavior stabilizes after 120 pulses at 1810 ± 90 °C. The optimized mock-up shows constant surface temperatures of 1630 ± 80 °C throughout all applied 500 pulses.

Fig. 15 shows thermographic and optical images of the heuristic mock-up during cycling at 130 °C coolant temperature. At the start of the procedure, the temperature distribution across all armor tiles is homogeneous. Hot spots develop and increase in intensity from the first pulses until the 120th pulse and stabilize after that.

After high heat flux testing, the mock-ups are cut in the longitudinal and transversal directions as marked in Fig. 16 to prepare metallographic microsections. The samples are etched with freshly prepared Murakamiś reagent (10 g NaOH, 10 g $K_3[(CN)_6]$, 100 g H_2O). The post-exposure microsection of the heuristic mock-up can be seen in Fig. 17. The transversal microsection shows a crack in the W armor tiles corresponding to one of the hotspots seen in Fig. 15. This cracking behavior is attributed to the effects of the anisotropic fracture properties of W plate material, e.g. described in [21] in the context of the ITER divertor PFCs. Directly above the crack, the sample shows significant grain growth due to the high temperatures in this part of the armor tile. The intact armor tiles also show grain growth, as can be seen in Fig. 17c.

Fig. 18 shows thermographic and optical images of the optimized mock-up during cycling. The mock-up shows no hot spots on the armor tiles. There is no visible difference in the surface temperatures of the first and the 500th pulse during cycling. From the start, some very small hot spots are localized between the armor tiles and at the bottom on the right side of the component. These hot spots are caused by leftovers from W foils, which were used to space out the W tiles during preform manufacturing. The heuristic mock-up does not have these spots because the armor tiles are directly cut from the build platform, so no spacing between tiles is necessary.

The post-exposure microsections of the optimized mock-up are shown in Fig. 19. The transversal cut shows some comparably large pores in the Cu matrix localized between the individual sections of the honeycomb lattice structure. Even though the pores formed directly beneath the armor tiles during infiltration, they are not detectable as hot spots in the thermographic imaging during HHF testing. However, the maximum surface temperature of the optimized mock-up is measured to be higher than that of the heuristic sample. This behavior is also visible in the FE calculations, so the higher temperatures are attributed to the higher volume fraction of W at the material interface of the mock-up rather than the pores. The optimized mock-up shows one case of self-castellation [30], visible in the longitudinal cut of the sample in Fig. 19c. The armor tiles also experience some grain growth, but due to their lower surface temperature compared to the heuristic mock-up in cyclic testing, the grain growth is less pronounced as can be seen in Figs. 17b and 19b. The boundary of the grain growth visible in Fig. 19 (a) corresponds to the isotherms predicted by the FEM calculations shown in Fig. 13.

6. Conclusions and outlook

The present work investigates tailored W-Cu composites based on AM W preforms for use as heat sinks in PFCs. The behavior of such composites is investigated using high heat flux tests on PFC small-scale mock-ups. The results of two different mock-ups comprising different AM preforms are presented. One design is created using a heuristic

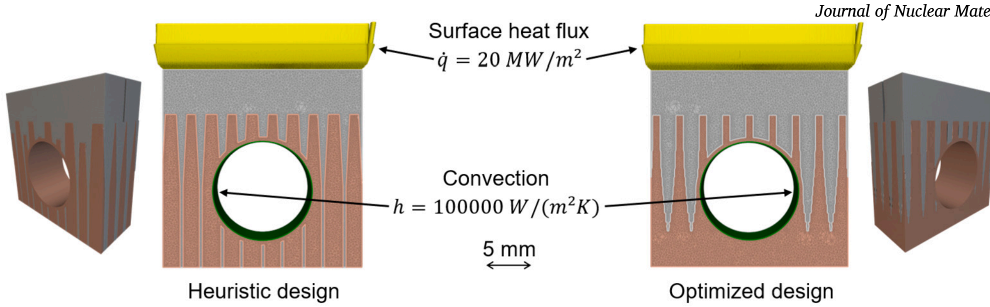

Fig. 12. Setup of the non-linear static thermal analysis in nTop 5.12.2 [28]. The width of the simulated area is 8.25 mm, according to 2 armor tiles and the castellation gap. The meshes were created with an edge length of 0.3 mm and a growth factor of 2. The temperature-dependent material data is taken from [29]. The thermal resistance between W and Cu is set to $1 \times 10^{-13}\ m^2\ K\ W^{-1}$. Radiative losses were neglected.

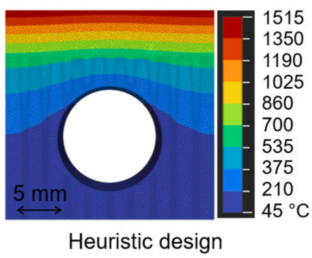

Fig. 13. Results of the non-linear static thermal analysis in nTop 5.12.2 for thermal equilibrium at $20\ MW\ m^{-2}$ and 20 °C coolant temperature. The maximum surface temperature of the heuristic design is calculated to be 1515 °C, while the maximum surface of the optimized design is calculated to be 1595 °C.

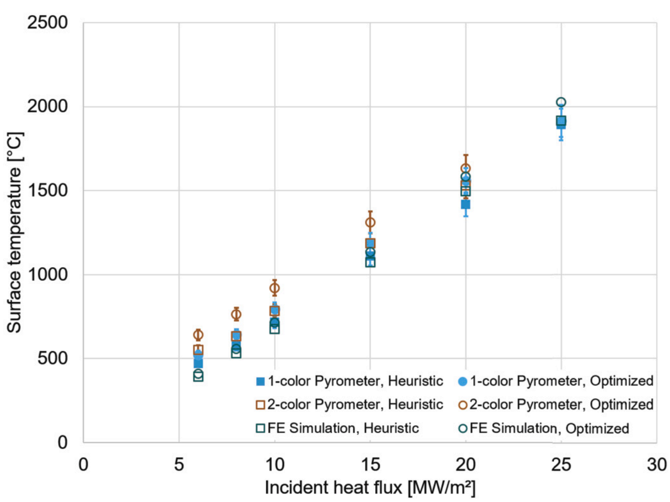

Fig. 14. Surface temperatures during screening with 20 °C cooling water of both tested mock-ups. Both samples show a linear increase of surface temperature with incident heat flux. The optimized mock-up shows slightly higher surface temperatures than the heuristic mock-up. This behavior is replicated in the results of the FE simulations.

design approach, and the second one is designed utilizing a finite element analysis to minimize peak thermally induced von Mises stresses by optimizing the W-Cu material distribution in the heat sink part. Both designs show comparable surface temperatures at various incident heat fluxes, ranging from $6\ MW\ m^{-2}$ to $25\ MW\ m^{-2}$. The optimized design shows slightly higher surface temperatures at all heat flux levels than the heuristic design. This behavior is consistent with accompanying FEM calculations. However, the heuristic design develops hot spots during cyclic testing up to 500 pulses at $20\ MW\ m^{-2}$ and hot water cooling conditions. The location of the hot spots corresponds to the locations of cracks in the armor tiles found during metallographic analysis. The cracks are attributed to the anisotropic cracking behavior of rolled W and the misalignment of the rolling direction of the W armor tiles and the heat flux direction as described in [21]. The overheated regions experience extensive grain growth. The optimized mock-up shows stable surface temperatures of 1660 ± 85 °C throughout all 500 pulses at $20\ MW\ m^{-2}$ without any hot spots. From these results, we draw the following conclusions:

- Even though the material quality of the samples is sub-optimal, the mock-ups still showed very promising performance during cyclic high heat flux testing.
- The composite material utilizing AM preforms and subsequent melt infiltration shows a high-integrity material joint between the W armor tile and the Cu heat sink.
- During the high heat flux tests performed in this work, no failure of the composite heat sink is observed, which confirms the potential of such an MMC for the use in plasma-facing components.
- Since the difference in surface temperature during the screening procedure is reproducible with FE calculations, the MMC PFC design is suspected to be resilient against the formation of pores in the matrix phase.

As a consequence, this work shows that tailored W-Cu composite heat sinks are a viable option for highly heat-loaded plasma-facing components. However, some open questions have to be investigated in the future. Most importantly, the material quality of the AM W and the infiltrated Cu matrix needs to be improved. Furthermore, the full potential of the optimization should be leveraged by choosing a different lattice type, e.g., a body-centered cubic type, exploiting more sophisticated preform and composite architectures, as well as optimized cooling channel geometries. Also, the cost function of the *MSPFC* code could include more components, for example, a term for a minimal surface temperature.

CRediT authorship contribution statement

R. Lürbke: Visualization, Methodology, Investigation, Formal analysis, Conceptualization. **A. von Müller:** Writing – review & editing, Supervision, Methodology, Conceptualization. **B. Böswirth:** Writing – review & editing, Investigation, Formal analysis. **B. Curzadd:** Software, Investigation. **H. Greuner:** Writing – review & editing, Methodology, Investigation. **J. Riesch:** Writing – review & editing, Methodology, Investigation. **G. Schlick:** Writing – review & editing, Supervision, Methodology, Conceptualization. **R. Neu:** Writing – review & editing, Supervision, Project administration, Funding acquisition.

Declaration of competing interest

The authors declare that they have no known competing financial interests or personal relationships that could have appeared to influence the work reported in this paper.

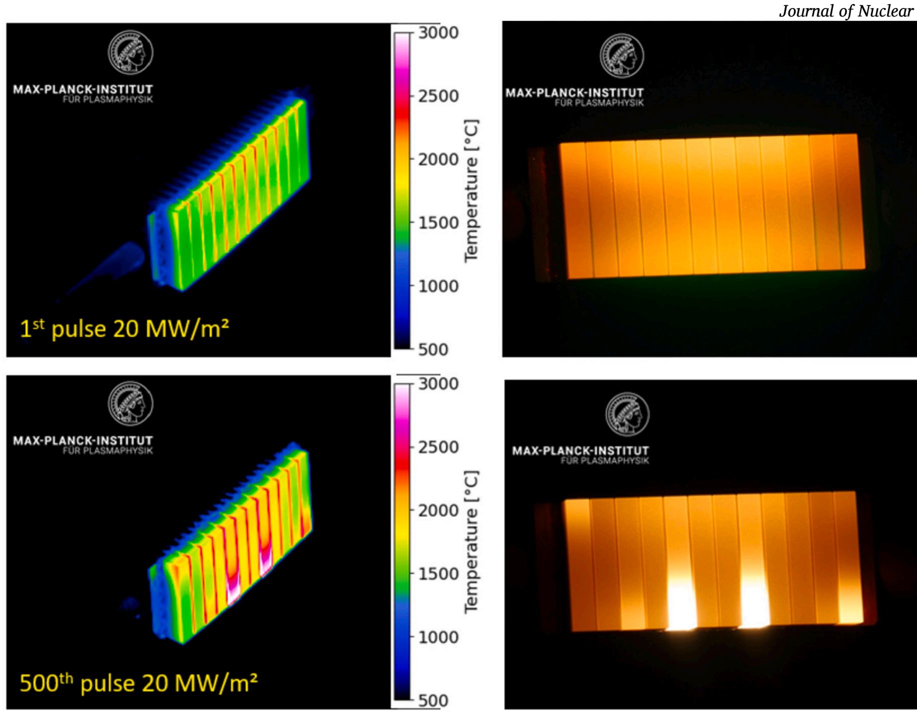

Fig. 15. Thermographic and optical imaging of the heuristic mock-up during cyclic loading. At the first pulse, the temperature distribution was homogeneous. The hot spots at the edge of the tiles developed quickly during testing but stabilized after 120 pulses.

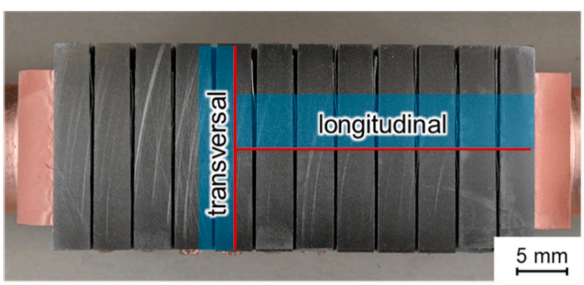

Fig. 16. Cutting schematic for the metallographic microsections in the transversal and longitudinal directions. The red lines mark the cutting line, and the blue areas mark the prepared sections of the sample. (For interpretation of the colors in the figure(s), the reader is referred to the web version of this article.)

Acknowledgements

The authors thank Patrick Junghanns for his support with his knowledge of processing and machining.

This work has been carried out within the framework of the EUROfusion Consortium, funded by the European Union via the Euratom Research and Training Programme (Grant Agreement No 101052200 - EUROfusion). Views and opinions are however those of the author(s) and do not necessarily reflect those of the European Union or the European Commission. Neither the European Union nor the European Commission can be held responsible for them.

Statement: During the preparation of this work the authors used Grammarly and DeepL in order to improve the language and writing of this work. After using this tool/service, the authors reviewed and edited the content as needed and take full responsibility for the content of the publication.

Data availability

Data will be made available on request.

References

[1] T. Donné, W. Morris, X. Litaudon, C. Hidalgo, D. McDonald, H. Zohm, E. Diegele, A. Möslang, K. Nordlund, G. Federici, P. Sonato, C. Waldon, D. Borba, P. Helander, European research roadmap to the realisation of fusion energy, https://euro-fusion.org/eurofusion/roadmap/, 2018.

[2] H. Zohm, Assessment of DEMO challenges in technology and physics, Fusion Eng. Des. 88 (6) (2013) 428–433, https://doi.org/10.1016/j.fusengdes.2013.01.001, https://www.sciencedirect.com/science/article/pii/S0920379613000021.

[3] IAEA, ITER Technical Basis, Text, International Atomic Energy Agency, publication Title: ITER Technical Basis, https://www.iaea.org/publications/6492/iter-technical-basis, 2002.

[4] H. Bolt, V. Barabash, W. Krauss, J. Linke, R. Neu, S. Suzuki, N. Yoshida, ASDEX Upgrade Team, Materials for the plasma-facing components of fusion reactors, J. Nucl. Mater. 329–333 (2004) 66–73, https://doi.org/10.1016/j.jnucmat.2004.04.005, https://www.sciencedirect.com/science/article/pii/S0022311504001242.

[5] R. Neu, J.W. Coenen, B. Curzadd, H. Gietl, H. Greuner, T. Höschen, K. Hunger, R. Lürbke, A. Müller, J. Riesch, G. Schlick, U. Siefken, E. Visca, J.H. You, Material and component developments for the DEMO divertor using fibre reinforcement and additive manufacturing, Mater. Res. Express 10 (11) (2023) 116516, https://doi.org/10.1088/2053-1591/ad0c7c.

[6] M. Merola, W. Dänner, M. Pick, EU R&D on divertor components, Fusion Eng. Des. 75–79 (2005) 325–331, https://doi.org/10.1016/j.fusengdes.2005.06.139, https://www.sciencedirect.com/science/article/pii/S0920379605002784.

[7] M. Roedig, W. Kuehnlein, J. Linke, M. Merola, E. Rigal, B. Schedler, E. Visca, Investigation of tungsten alloys as plasma facing materials for the ITER divertor, Fusion Eng. Des. 61–62 (2002) 135–140, https://doi.org/10.1016/S0920-3796(02)00113-8, https://www.sciencedirect.com/science/article/pii/S0920379602001138.

[8] M. Rödig, R. Duwe, W. Kühnlein, J. Linke, M. Merola, B. Schedler, G. Vieider, E. Visca, Reference testing of actively cooled mock-ups for the neutron-irradiation experiments PARIDE 3 and 4, Fusion Eng. Des. 56–57 (2001) 417–420, https://doi.org/10.1016/S0920-3796(01)00345-3.

[9] E. Visca, S. Libera, A. Mancini, G. Mazzone, A. Pizzuto, C. Testani, Hot radial pressing: an alternative technique for the manufacturing of plasma-facing components, Fusion Eng. Des. 75–79 (2005) 485–489, https://doi.org/10.1016/j.fusengdes.2005.06.123, https://www.sciencedirect.com/science/article/pii/S0920379605002553.

[10] F. Crescenzi, S. Roccella, E. Visca, A. Moriani, Comparison between FEM and high heat flux thermal fatigue testing results of ITER divertor plasma facing mock-ups, Fusion Eng. Des. 89 (7) (2014) 985–990, https://doi.org/10.1016/j.fusengdes.2014.04.012, https://www.sciencedirect.com/science/article/pii/S0920379614002890.

[11] M. Li, J.-H. You, Interpretation of the deep cracking phenomenon of tungsten monoblock targets observed in high-heat-flux fatigue tests at 20 MW/m 2, Fusion Eng. Des. 101 (2015) 1–8, https://doi.org/10.1016/j.fusengdes.2015.09.008, https://linkinghub.elsevier.com/retrieve/pii/S0920379615302775.

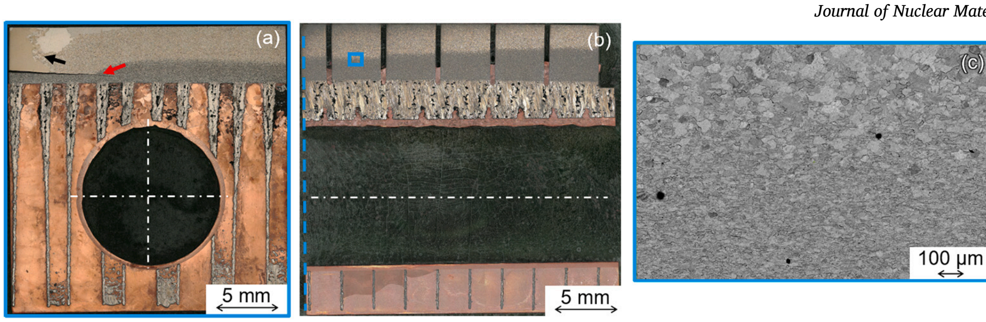

Fig. 17. Metallographic microsections of the heuristic mock-up after high heat flux testing. The lighter areas of the armor tiles have experienced grain growth. **(a)** Transversal cut. The crack indicated by the red arrow corresponds to the left overheated tile in Fig. 15. The armor tile experienced grain growth above the crack, as indicated by the black arrow. The Cu matrix shows some small pores close to the armor tiles. **(b)** Longitudinal cut. The AM W shows a large number of pores. **(c)** Enlarged view of one of the armor tiles, showing grain growth.

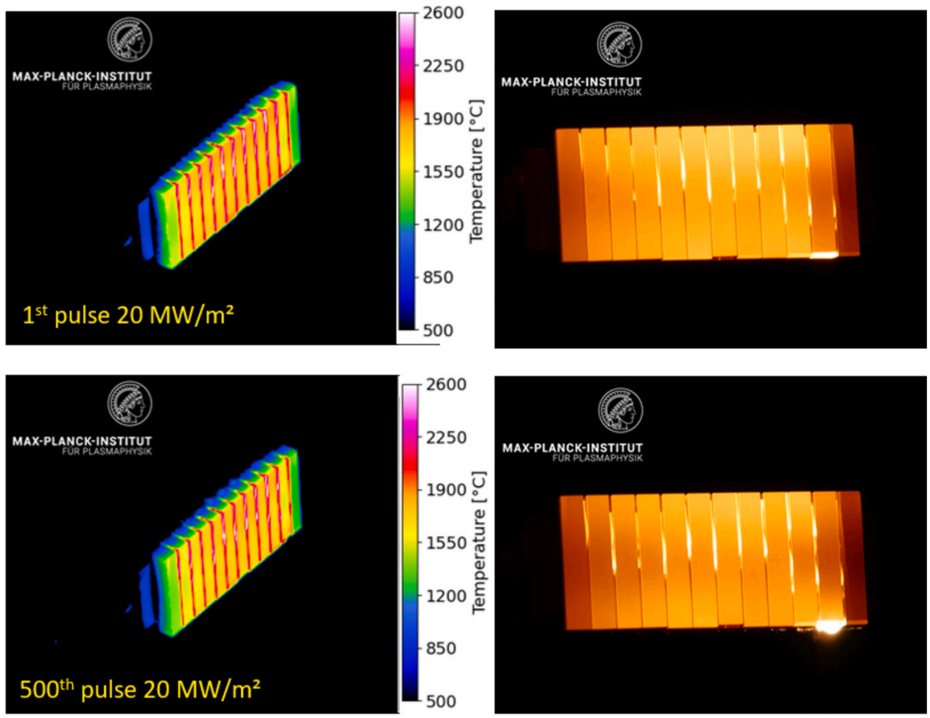

Fig. 18. Thermography and optical imaging of the optimized mock-up during cyclic loading. The hot spots in the gaps of this sample are leftovers from W foils used as spacers for manufacturing. There is no observable change in the performance of the PFC between the first and the 500th pulse.

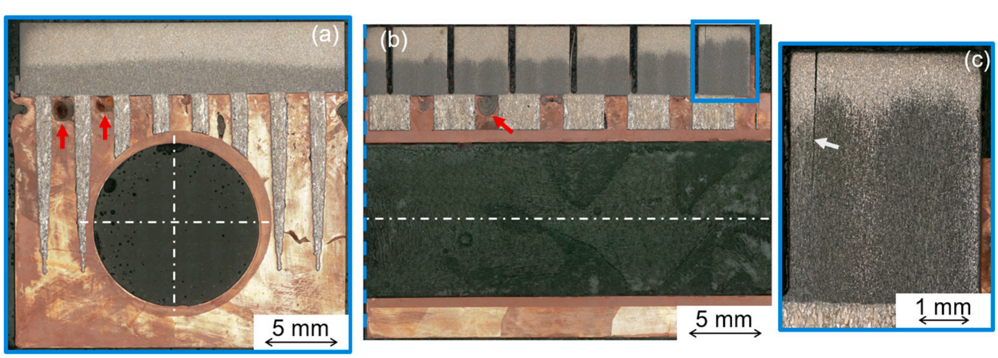

Fig. 19. Metallographic microsections of the optimized mock-up after high heat flux testing. The lighter areas of the armor tiles have experienced grain growth. **(a)** Transversal cut. The infiltration of this sample formed macroscopic pores between the individual sections of the honeycomb lattice, indicated by the red arrows. **(b)** Longitudinal cut. The pores formed directly underneath the armor tiles (red arrow). **(c)** Enlarged view of one of the armor tiles. The tile shows self-castellation [30] after testing, indicated by the white arrow. The armor tile experienced grain growth during testing.

[12] G. Pintsuk, I. Bobin-Vastra, S. Constans, P. Gavila, M. Rödig, B. Riccardi, Qualification and post-mortem characterization of tungsten mock-ups exposed to cyclic high heat flux loading, Fusion Eng. Des. 88 (9–10) (2013) 1858–1861, https://doi.org/10.1016/j.fusengdes.2013.05.091.

[13] D. Munz, Y.Y. Yang, Stress singularities at the interface in bonded dissimilar materials under mechanical and thermal loading, J. Appl. Mech. 59 (4) (1992) 857–861, https://doi.org/10.1115/1.2894053, https://asmedigitalcollection.asme.org/appliedmechanics/article/59/4/857/389664/Stress-Singularities-at-the-Interface-in-Bonded.

[14] D. Munz, Y. Yang, Stresses near the free edge of the interface in ceramic-to-metal joints, J. Eur. Ceram. Soc. 13 (5) (1994) 453–460, https://doi.org/10.1016/0955-2219(94)90024-8, https://linkinghub.elsevier.com/retrieve/pii/0955221994900248.

[15] J. You, H. Bolt, Analysis of singular interface stresses in dissimilar material joints for plasma facing components, J. Nucl. Mater. 299 (1) (2001) 1–8, https://doi.org/10.1016/S0022-3115(01)00680-8, https://linkinghub.elsevier.com/retrieve/pii/S0022311501006808.

[16] M. Diez, Y. Corre, E. Delmas, N. Fedorczak, M. Firdaouss, A. Grosjean, J.P. Gunn, T. Loarer, M. Missirlian, M. Richou, E. Tsitrone, t.W. Team, In situ observation of tungsten plasma-facing components after the first phase of operation of the WEST tokamak, Nucl. Fusion 61 (10) (2021) 106011, https://doi.org/10.1088/1741-4326/ac1dc6.

[17] B. Curzadd, A. Von Müller, R. Neu, U. Von Toussaint, Topology optimization of tungsten/copper structures for plasma-facing component applications, Nucl. Fusion 59 (8) (2019) 086003, https://doi.org/10.1088/1741-4326/ab1ff5, https://iopscience.iop.org/article/10.1088/1741-4326/ab1ff5.

[18] DIN, Additive Fertigung - Grundlagen - Terminologie (ISO/ASTM 52900:2021); Deutsche Fassung, Tech. rep., Beuth Verlag GmbH, 2021, https://doi.org/10.31030/3290011, https://www.beuth.de/de/-/-/344258696.

[19] A. Müller, D. Dorow-Gerspach, M. Balden, M. Binder, B. Buschmann, B. Curzadd, T. Loewenhoff, R. Neu, G. Schlick, J. You, Progress in additive manufacturing of pure tungsten for plasma-facing component applications, J. Nucl. Mater. 566 (2022) 153760, https://doi.org/10.1016/j.jnucmat.2022.153760, https://linkinghub.elsevier.com/retrieve/pii/S0022311522002471.

[20] Tekna Advanced Materials Inc., Material test certifiacte Tekmat W-25 (Oct. 2022).

[21] T. Hirai, F. Escourbiac, V. Barabash, A. Durocher, A. Fedosov, L. Ferrand, T. Jokinen, V. Komarov, M. Merola, S. Carpentier-Chouchana, N. Arkhipov, V. Kuznetcov, A. Volodin, S. Suzuki, K. Ezato, Y. Seki, B. Riccardi, M. Bednarek, P. Gavila, Status of technology R&D for the ITER tungsten divertor monoblock, J. Nucl. Mater. 463 (2015) 1248–1251, https://doi.org/10.1016/j.jnucmat.2014.12.027, https://www.sciencedirect.com/science/article/pii/S0022311514009696.

[22] A. Feichtmayer, Experimentelle Charakterisierung von Wolfram-Kupfer-Verbundwerkstoffen auf Basis additiv hergestellter Vorformen, Master's thesis, Technische Universität München, München, 2021.

[23] H. Greuner, H. Bolt, B. Böswirth, T. Franke, P. McNeely, S. Obermayer, N. Rust, R. Süß, Design, performance and construction of a 2 MW ion beam test facility for plasma facing components, Fusion Eng. Des. 75–79 (2005) 345–350, https://doi.org/10.1016/j.fusengdes.2005.06.021, https://www.sciencedirect.com/science/article/pii/S0920379605001006.

[24] H. Greuner, B. Boeswirth, J. Boscary, P. McNeely, P. McNeely, High heat flux facility GLADIS: operational characteristics and results of W7-X pre-series target tests, J. Nucl. Mater. 367 (2007) 41992330, https://doi.org/10.1016/j.jnucmat.2007.04.004.

[25] R.A. Pitts, S. Bardin, B. Bazylev, M.A. van den Berg, P. Bunting, S. Carpentier-Chouchana, J.W. Coenen, Y. Corre, R. Dejarnac, F. Escourbiac, J. Gaspar, J.P. Gunn, T. Hirai, S.-H. Hong, J. Horacek, D. Iglesias, M. Komm, K. Krieger, C. Lasnier, G.F. Matthews, T.W. Morgan, S. Panayotis, S. Pestchanyi, A. Podolnik, R.E. Nygren, D.L. Rudakov, G. De Temmerman, P. Vondracek, J.G. Watkins, Physics conclusions in support of ITER W divertor monoblock shaping, Nucl. Mater. Energy 12 (2017) 60–74, https://doi.org/10.1016/j.nme.2017.03.005, https://www.sciencedirect.com/science/article/pii/S2352179116302885.

[26] J.-H. You, E. Visca, T. Barrett, B. Böswirth, F. Crescenzi, F. Domptail, G. Dose, M. Fursdon, F. Gallay, H. Greuner, K. Hunger, A. Lukenskas, A. von Müller, M. Richou, S. Roccella, C. Vorpahl, K. Zhang, High-heat-flux technologies for the European DEMO divertor targets: state-of-the-art and a review of the latest testing campaign, J. Nucl. Mater. 544 (2020) 152670, https://doi.org/10.1016/j.jnucmat.2020.152670.

[27] Y. Bournonville, M. Grandotto, S. Pascal-Ribot, P. Spitz, F. Escourbiac, Numerical simulation of swirl-tube cooling concept, application to the ITER project, Fusion Eng. Des. 84 (2) (2009) 501–504, https://doi.org/10.1016/j.fusengdes.2008.11.028, https://www.sciencedirect.com/science/article/pii/S0920379608003530.

[28] nTop | Computational Design Software | formerly nTopology, https://www.ntop.com/.

[29] A. Alekseev, R. Atroshenkov, V. Barabash, B. Baragano, D. Couso, G. Dellopoulos, J. Fano, B. Fernández, E. Fernandez, F. Fernández, J. Guirao, G. Kalinin, S. Kang, S. Khomiakov, J.L. Lastra, V.J. Martínez, A. Obushev, J. Ordieres, A. Portone, G. Sannazzaro, I. Vázquez, L. Villabrille, I. Zatz, Structural Design Criteria for ITER In-vessel Components, Tech. rep., ITER Organization, 2012.

[30] S. Panayotis, T. Hirai, V. Barabash, A. Durocher, F. Escourbiac, J. Linke, T. Loewenhoff, M. Merola, G. Pintsuk, I. Uytdenhouwen, M. Wirtz, Self-castellation of tungsten monoblock under high heat flux loading and impact of material properties, Nucl. Mater. Energy 12 (2017) 200–204, https://doi.org/10.1016/j.nme.2016.10.025, https://www.sciencedirect.com/science/article/pii/S2352179116300874.